Mon. Not. R. astr. Soc. (1983) **202,** 125–143

MR 2251 – 178: a nearby QSO embedded in a giant H II envelope

J. Bergeron★ *Institut d'Astrophysique, 98 bis, Boulevard Arago, F-75014 Paris, France*

A. Boksenberg *Royal Greenwich Observatory, Herstmonceux Castle, Hailsham, East Sussex BN27 1RP*

M. Dennefeld★ *Institut d'Astrophysique, 98 bis, Boulevard, Arago, F-75014 Paris, France*

M. Tarenghi *European Southern Observatory, Karl Schwarzschild Strasse 2, D-8046 Garching bei München, Germany*

Received 1982 March 31; in original form 1981 August 11

Summary. The nearby QSO MR 2251–178 photographically shows a surrounding nebulosity of diameter ~27 kpc ($H_0 = 50\,\mathrm{km\,s^{-1}\,Mpc^{-1}}$). Our spatially resolved spectrophotometry of the QSO and surrounding field reveals that the QSO lies in the nucleus of a galaxy having a gaseous component of very high ionization, high temperature ($T = 3 \times 10^4$ K) and relatively low abundance and is surrounded by a giant H II envelope which we observe in [O III] emission. The ionized matter in the envelope extends over a region of at least 230 × 60 kpc and is not associated with any nebulosity apparent on broad-band photographic plates; its velocity field resembles those of observed H I envelopes. A clear rotation pattern is seen close to the QSO with a velocity gradient of $17\,\mathrm{km\,s^{-1}\,kpc^{-1}}$ out to 6 kpc. At large distances from the QSO nucleus, $50 < r < 170$ kpc in the south-east direction, the rotation curve is flat. The total mass of MR 2251–178 within a radius of 170 kpc is $(1.3 \times 10^{12}/\sin^2 i) M_\odot$. The hard radiation energy source can easily power the whole envelope. From the ionization equilibrium we derive an upper limit of $0.2\,\mathrm{cm^{-3}}$ for the density in the envelope and the mass of ionized gas is $2 \times 10^{10} < M_{\mathrm{H\,II}} < 5 \times 10^{11} M_\odot$. The upper limit on the ratio $M_{\mathrm{H\,II}}/M_{\mathrm{total}}$ is 0.25 and if stars are associated with the giant envelope they must be very faint in the optical. We confirm that the QSO lies in the outskirts of a small cluster of galaxies. The mass of the H II envelope (observed extent) is smaller than the mass of hot X-ray emitting gas often present in clusters of galaxies. A second, background, cluster seems also to be present, at a redshift $z = 0.12$.

★The observations and data analysis were carried out while the authors were part of the ESO scientific group.

1 Introduction

The nearby QSO MR 2251 − 178 was the first to be discovered from X-ray observations (Cooke *et al.* 1978; Ricker *et al.* 1978; Ricker *et al.* 1979). It is a strong X-ray source [L_x(2–10 keV) ~ 1×10^{45} erg s^{-1}] and has been reported to vary by a factor of about 10 (Cooke *et al.* 1978). Its optical spectrum closely resembles those of other low-redshift QSOs (Canizares, McClintock & Ricker 1978) and it has been observed to vary optically on time-scales from one month to about one year (Ricker *et al.* 1979). At its observed peak X-ray brightness the ratio of X-ray-to-optical luminosity is ~3:1 (Ricker *et al.* 1979), somewhat higher than for 3C 273 which has ~1:1 (Worrall *et al.* 1980). Finally, it is a weak, pointlike radio source (Ricker *et al.* 1978).

Although Ricker *et al.* (1978) first described MR 2251−178 as being stellar in appearance on Palomar Observatory Sky Survey plates, subsequent deep photography revealed a clear nebulosity surrounding a stellar core (Ricker *et al.* 1979; Phillips 1980). Further, the QSO is apparently within the boundary of a loose, irregular cluster of galaxies (Phillips 1980) whose sizes are consistent with a distance derived from the QSO redshift. The closest of these to the QSO (galaxy 1) was found by Ricker *et al.* (1978) to coincide with an extended radio source of very low surface brightness. From spectrophotometry of four of the galaxies, including galaxy 1, Phillips (1980) found it very likely that the QSO indeed was a member of the cluster although its radial velocity was somewhat lower than for the galaxies measured. Earlier, and conflicting, results by Fairall (1979) from more meagre data denied such an association.

Nebulosity in association with QSOs is now consistently observed (Kristian 1973; Wyckoff, Wehinger & Gehren 1981) and emission lines have been found in several cases, e.g.: 3C 48 (Wampler *et al.* 1975), 4C 37.43 (Stockton 1976), 3C 206 (Wyckoff *et al.* 1980a) and 3C 273 (Wyckoff *et al.* 1980b). Wyckoff *et al.* (1980a) also found evidence for a stellar populations in the nebulosity of 3C 206 and identified an associated cluster of galaxies. Associated galaxies also have been found for several other QSOs (e.g. Gunn 1971; Stockton 1978).

We independently noticed the non-stellar character of MR 2251−178 and also the surrounding cluster of galaxies. The QSO appears somewhat similar to the Seyfert 1 galaxy 3C 120 although twice as distant and more luminous. Within the nebulosity of 3C 120 Baldwin *et al.* (1980) showed the existence of a stellar population and an extensive network of H II regions of high-ionization level. Here we report our observations of MR 2251−178, which we undertook in the context of a survey of bright Seyfert 1 galaxies aimed at understanding the interaction between active nuclei and their surrounding discs or nebulosities; we included several of the surrounding galaxies to check their association with the QSO. We report also the incidental discovery of an associated giant H II envelope not evident as nebulosity on direct photographs.

2 Observations

A direct plate (IIIa-J emulsion + GG 385 filter) of the field of MR 2251−178 was obtained on the night of 1979 September 7 (UT) using the triplet corrector at the prime focus of the ESO 3.6-m telescope at La Silla. A reproduction from this plate is given in Plate 1.

We obtained spectra of the QSO, its surrounding field and six galaxies of the cluster (G1–G6 in Plate 1) on the nights of 1978 September 5, 6 and 9 (UT) with the Boller & Chivens spectrograph and the University College London Image Photon Counting System (Boksenberg 1978) on the ESO 3.6-m telescope. The air-mass was always small, from 1.03 to 1.20. We used an image format of the 1500 spectral elements by 72 spatial increments each of 1.76 arcsec along the slit. A dispersion of 114 Å mm^{-1} in first order gave

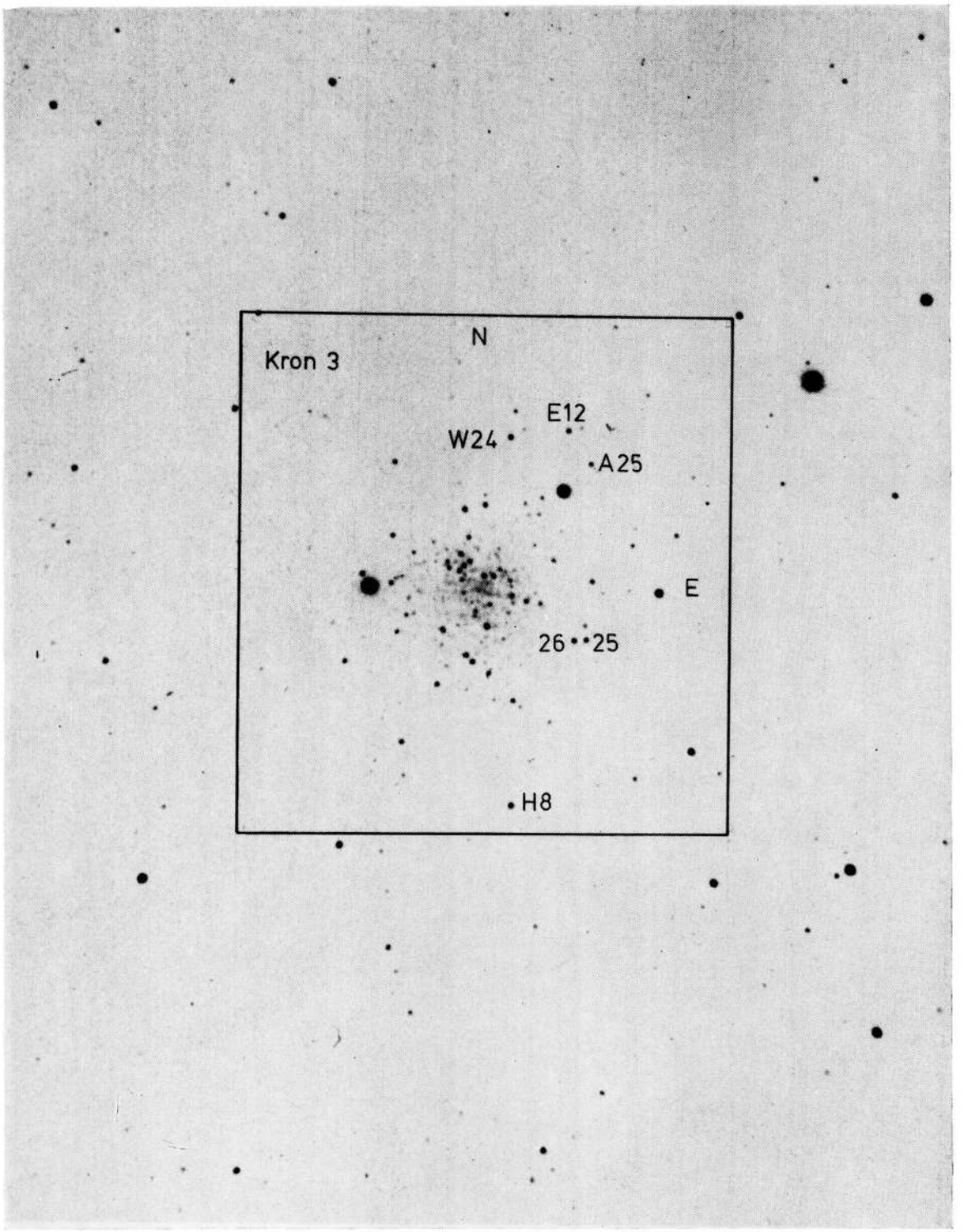

Plate 1. Finding chart (*V* Plate) for cluster Kron 3. The numbers are from Gascoigne (to be published).

[*facing page* 60]

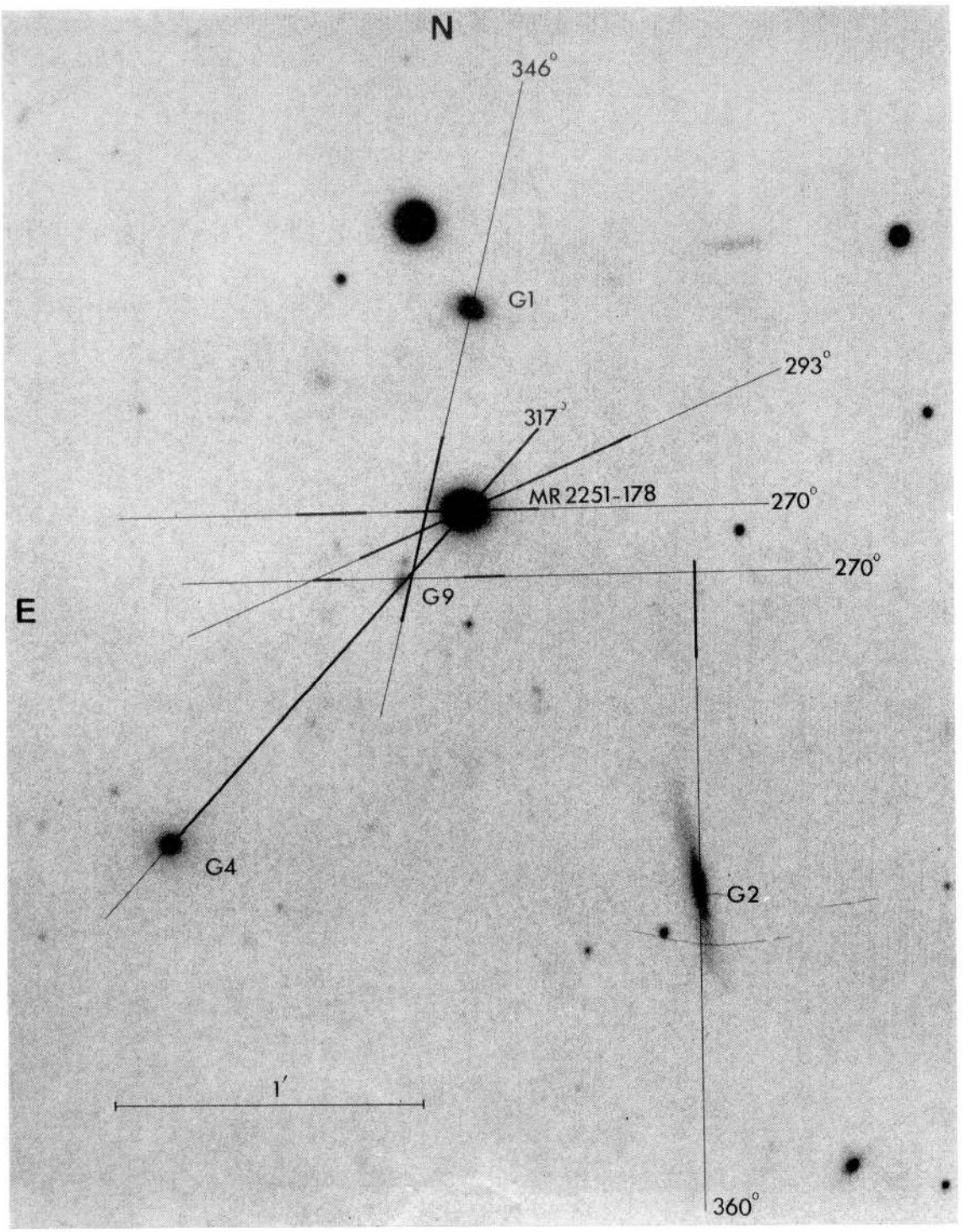

Plate 2. Enlargement of the plate shown in Plate 1. Slit positions close to the QSO are indicated in extent and labelled with the position angle. Regions where we detect [O III] emission are indicated by a thick continuous line.

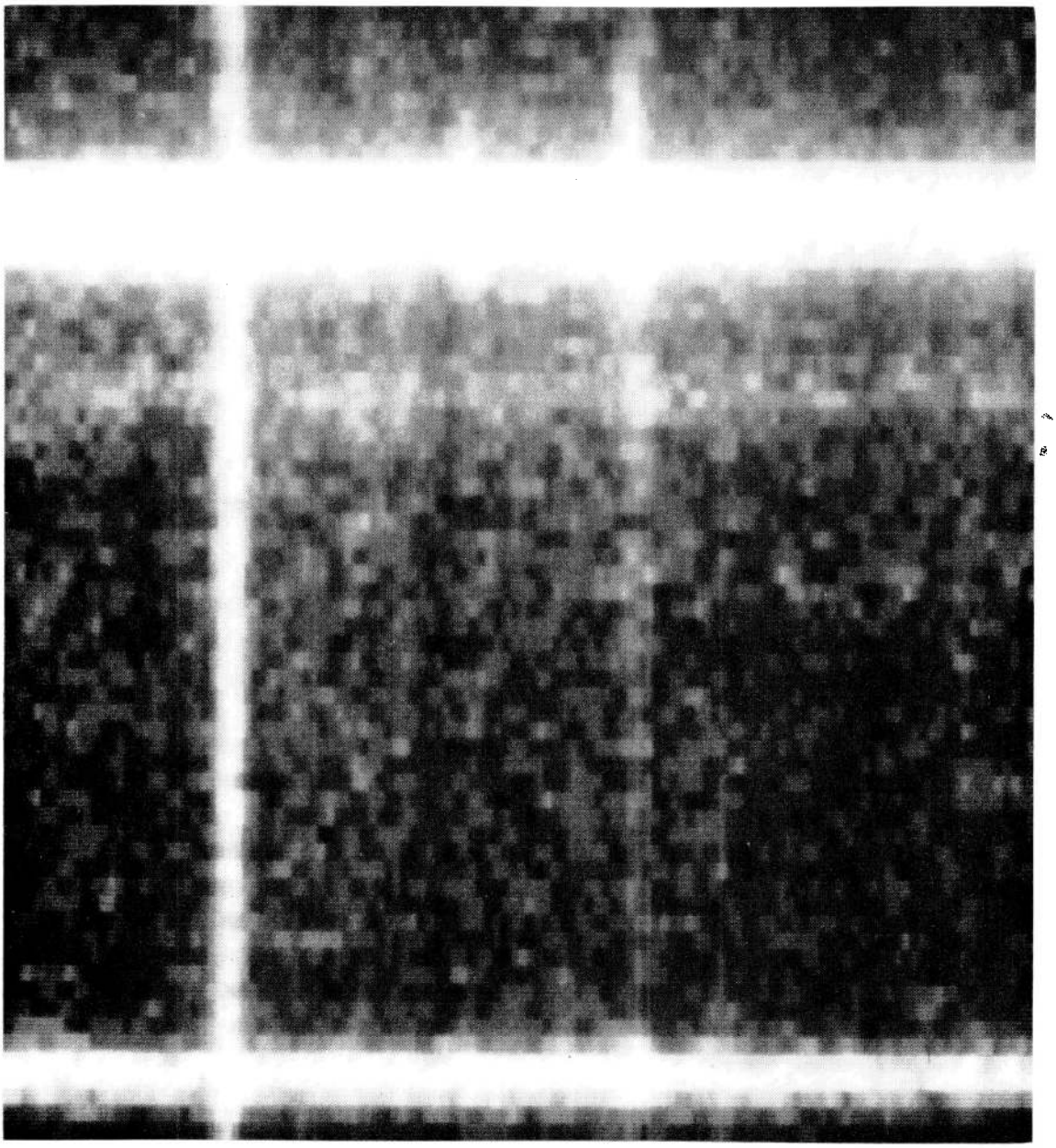

Plate 3. Section of a two-dimensional spectrum showing the extended H II envelope associated with MR 2251−178, obtained with the IPCS and a slit at position angle 317° (see Plate 2). The night sky line λ5199 (left) is included with the redshifted [O III] lines. Each horizontal strip covers 1.76 arcsec or 3.3 kpc at the QSO ($H_0 = 50$ km s^{-1} Mpc^{-1}). The brighter continuum at the top comes from the QSO and the one at the bottom from the south-east galaxy G4. The faint continuum just below that of the QSO comes from the background galaxy at $z=0.121$. The spectrum was photographed from a TV monitor.

1983MNRAS.202..125B

enough coverage to include lines of elements in several stages of ionization in one exposure. Details of the observations are given in Table 1. The slit width was set at 3 arcsec in moderate seeing and 2 arcsec in good seeing. Each exposure on the field was followed by a short exposure on a comparison arc. The slit positions used in the close neighbourhood of the QSO are shown in Plate 2. Of these, three include the QSO nucleus at position angles 270°, 293° and 317°. Because of the pervasion of [O III] emission we found in this region we made separate exposures on empty fields near the QSO position to allow subtraction of the sky component from the spectral arrays. Subsequently, on the nights of 1978 November 23 and 24 we obtained spectra of two more galaxies (G7 and G8 in Plate 1) with the ESO

Table 1. Journal of observations.

Date (UT)	Detector	Object ★	Position Angle (°)	Wavelength Range (Å)	Slitwidth (")	Instrumental FWHM (Å)	Integration Time (minutes)	Remarks
1978								
Sep. 5	IPCS	MR 2251-178 G9 G4 envelope	317	3570-7220	3.0	7.0	36	Cloudy
"	"	G2 emission region	360	3570-7225	"	"	36.5	"
"	"	G1 nebulosity envelope	346	"	"	"	68	"
"	"	12" south QSO G9 envelope	270	"	"	"	17	"
"	"	MR 2251-178 envelope	293	"	2.0	5.5	24	"
Sep. 6	"	G3 G5	310	3645-7210	3.0	7.0	12	"
"	"	G6	270	"	"	"	"	"
"	"	MR 2251-178 envelope	"	"	1.0	4.0	10	"
Sep. 9	"	MR 2251-178 envelope	"	5000-7690	2.0	5.5	33	
"	"	G1	"	"	"	"	23	
1979								
Nov. 23	IDS	G7	"	3800-7100	1.0	16	20	
Nov. 24	"	G8	"	"	"	"	"	

★ Observation of the nebulosity always accompanies MR 2251-178

Image Dissector Scanner in place of the IPCS. Details of these observations are also given in Table 1. Photometric calibrations were made from associated observations of standard stars (Oke 1974), although the nights were not of photometric quality. For the QSO, second order contamination of the spectrum $> \lambda 6000$ was large and an additional exposure was made using a GG 495 filter to suppress the blue region.

The data were reduced with the Image Handling and Processing software developed at ESO. For our velocity analyses, line positions and widths were obtained by fitting Gaussian profiles to the observed lines. The uncertainty in our wavelength determination is indicated by the dispersion in our measurements of the position of the $\lambda 5577$ night sky line over a typical IPCS frame: ± 0.4 Å.

3 Results

From our direct photograph (Plates 1 and 2) we clearly see the QSO image to be non-stellar – the surrounding nebulosity extends greater than 15 arcsec in diameter – and that several of the surrounding galaxies show clear morphological structure (compare the photography of Ricker *et al.* 1979 and Phillips 1980). Our long-slit spectrophotometry reveals strong emission lines of high ionization in the vicinity of the QSO, corresponding to the nebulosity observed on the direct plate, but more striking is the existence of faint [O III] emission at very large distances from the QSO, for which an obvious counterpart is not apparent on the direct plate. In the section of one of our two-dimensional spectrograms represented in Plate 3 the [O III] $\lambda 5007$ line is seen to extend all the way to G4 (to avoid confusion we adopt the numeration of Phillips (1980) for galaxies 1–4), a distance of about 90 arcsec, or 170 kpc using the average cluster velocity derived from our measurements given in Table 2 and assuming $H_0 = 50\,\mathrm{km\,s^{-1}\,Mpc^{-1}}$.* The Balmer lines are not detected at large distances (> 20 kpc) from the QSO.

3.1 KINEMATICS OF THE EXTENDED REGION

We observe the extended region of emission over a total distance 230 kpc in the north-west to south-east direction and at least 60 kpc in the north-east to south-west direction (our mapping here is incomplete), as is indicated in Plate 2. In Fig. 1 we give [O III] $\lambda 5007$ intensity histograms for two of the slit positions passing through the QSO and the one at position angle 346° including the nebulosity. The line intensity is strongly peaked at the QSO nucleus and a gradual decrease in intensity by a factor about 40 occurs from the QSO ($r < 1.6$ kpc) to $r = 9.5$–13 kpc in the observed nebulosity and a further factor about 30 to $r > 45$ kpc in the extended emission region, where large spatial irregularities are evident particularly to the west of the nucleus. For $r < 30$ kpc both [O III] lines $\lambda\lambda 4959$ 5007 are clearly detected; from these we derive average velocities with an internal error $\sim \pm 20\,\mathrm{km\,s^{-1}}$. Such a good precision is achieved because of the line centring method used. At larger distances, with weaker emission, velocities can be derived from [O III] $\lambda 5007$ only, and we maintain a precision $\sim \pm 40\,\mathrm{km\,s^{-1}}$ by appropriately summing adjacent spectrum strips.

At large distances ($r > 50$ kpc) from the QSO the spread in average velocity of the emitting gas is small: $< 65\,\mathrm{km\,s^{-1}}$ over 100 kpc. Furthermore, at our resolution the [O III] $\lambda 5007$ line is only marginally resolved, if at all: in the whole of the extended emission region (including in the nebulosity) the full width at half maximum is at most 1.2 times greater than for the atmospheric line $\lambda 5577$ and we derive a maximum value for the FWHM radial velocity spread of the emitting gas of $200\,\mathrm{km\,s^{-1}}$. We shall see below that the

*We use this value throughout.

FWHM velocity spread of the surrounding cluster is much greater than the overall spread within the extended emitting gas.

For the slit positions passing through the QSO we observe clear rotation patterns centred on it, as shown in Fig. 2. In each case the precise location of the QSO along the slit was

Table 2. Optical lines of MR 2251 –178 and in the nebulosity.

	Identification[a]	MR 2251-178 Flux[b] (10^{-16} erg cm^{-2} s^{-1})	MR 2251-178 Observed EW (Å)	Nebulosity (r = 7") Flux[b] (10^{-16} erg cm^{-2} s^{-1})	Nebulosity (r = 7") Observed EW (Å)
3426	[Ne V]	470		34.0	31.2 ± 1.5
3444	O III	180			
3727	[O II]	735	9.7 ± 0.2	42.8	36.1 ± 1.5
3755	O III	82		5.5	
3869	[Ne III]	590		22.9	23.6 ± 1.0
3888	Hδ + He I	935			
3934	Ca II K (ab) z = 0.063				4.8 ± 0.8
3969	[Ne III] + Hε - Ca II H (ab)	485	8.8 ± 0.2	7.9	
4072	[S II]	220			
4102	Hδ (b)	710[c]			
4102	Hδ (n)	210[c]		6.9	
4244	[Fe II]	125			
4287	[Fe II]	155			
4340	Hγ (b)	2500[c]			
4340	Hγ (n)	590[c]		12.4	10.7 ± 0.5
4363	[O III]	840[c]		14.5	12.4 ± 0.5
4388	C III ?			2.5 :	
4471	He I (b)	possible			
4651	C III ?			5.9 :	
4686	He II (b)	1050[c]			
4686	He II (n)	135[c]	2.8 ± 0.2	9.5	6.8 ± 0.6
4861	Hβ (b)	8400[c]	226 ± 9		
4861	Hβ (n)	750[c]		23.1	13.9 ± 0.5
4959	[O III]	1560		77.9	51.0 ± 2.0
5007	[O III]	4370		230.0	152.0 ± 5.0
5060	[Fe III]			4.2 :	
5158	[Fe VII]	200			
5174	Mg I (ab) z = 0.063				4.1 ± 0.8
5276	[Fe VII]	190			
5876	He I (b)	2250	68 ± 2		
5876	He I (n)	70 :			
6086	[Fe VII]	250		14.0 :	
6300	[O I]	360	9.9 ± 0.5		
6364	[O I]	75			
6548	[N II]			11.0 :	
6563	Hα (b)	32000	1050 ± 50		
6563	Hα (n)	2230		87.0	34.0 :
6584	[N II]			21.0 :	
6717	[S II]	470		23.0 :	
6731	[S II]			17.0 :	
7006	[Ar V]	190			

[a] Broad (b) and narrow (n) components are listed separately.

[b] Fluxes have been corrected as described in the text. Systematic uncertainty dominates over statistical and possibly amounts to 50%. There is an additional uncertainty arising from placing the continuum, typically of order 5% for the broad line components and generally less for the narrow. The relative accuracy for nearby lines is of order a few per cent except in the more uncertain values indicated by a colon.

[c] Rough deblending only.

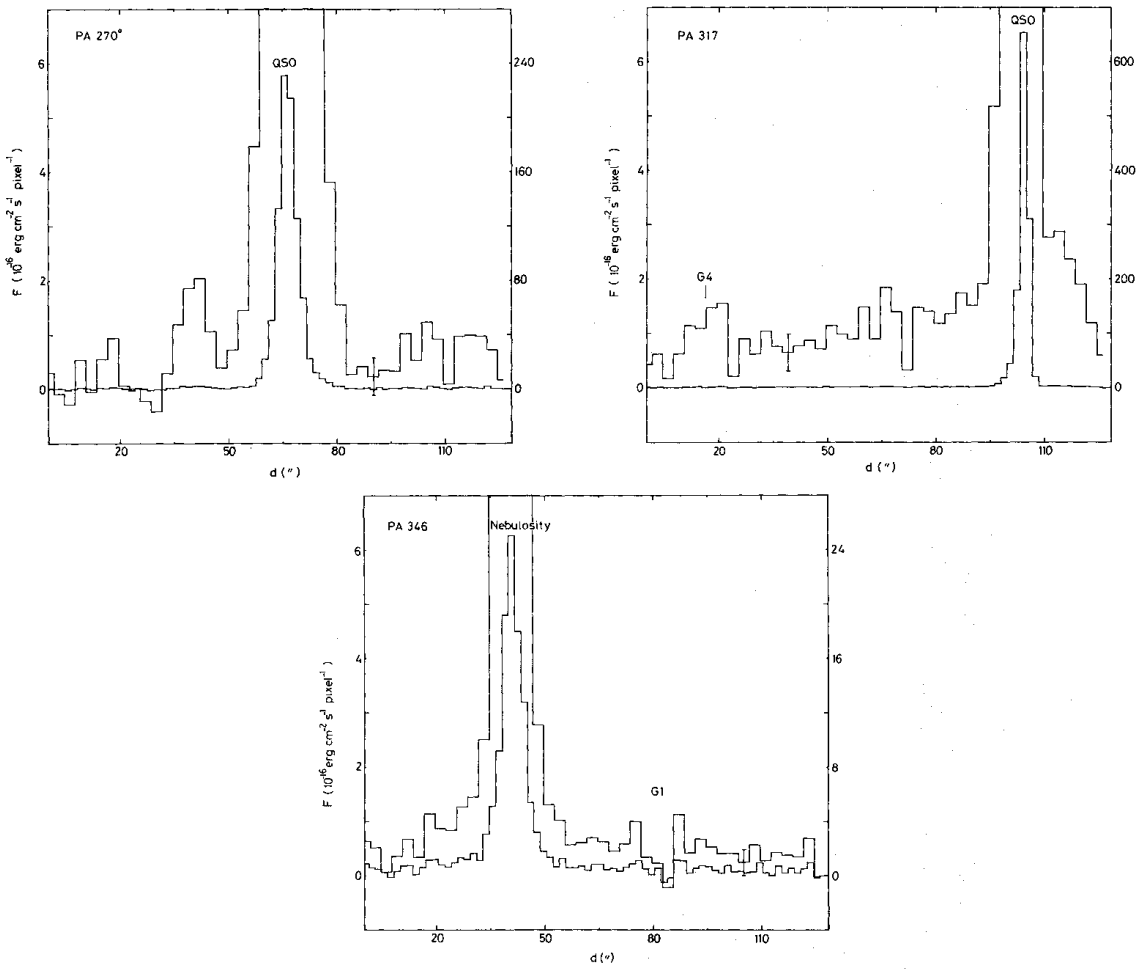

Figure 1. [O III] λ 5007 intensity histograms along the slit (distance d) passing through MR 2251 −178 at position angles 270° and 317° and through the nebulosity at position angle 346° and passing 7 arcsec from the QSO, all placed as indicated in Plate 2. The histograms are shown both at large scale (indicated right) and small scale (indicated left). A pixel has dimensions 3 arcsec across and 1.76 arcsec along the slit; the small scale histograms are smoothed by rebinning to 3 arcsec along the slit. Typical statistical (± 1σ) error bars are shown but systematic photometric uncertainties are not indicated. All data are photometrically corrected nominally as given in the text and with no attempt to make individual corrections; the differences apparent between the observed QSO profiles are due both to changes in photometric conditions and in seeing.

determined from an intensity histogram of the [O III] lines. The central velocity gradient is very similar for the three cases, 17 km s^{-1} kpc^{-1} out to $r = 6$ kpc, suggesting that the major axis of the rotating nebulosity has a position angle within our observed range 270° to 317°. This is consistent with the results from the slit position through G1 and passing close to the QSO (see plate 2).

The largest gaseous extension is observed in the south-east direction for the slit at position angle 317°. After a small dip near $r = 10$ kpc the rotation curve rises to a broad plateau with ~180 km s^{-1} relative to the QSO over the range $50 < r < 170$ kpc, or perhaps a broad maximum centred near 120 kpc; this can be seen in Fig. 3. We observed a similar trend in the south-east direction at position angle 293°, but for this case the rotation curve in the north-west direction flattens at $r > 25$ kpc with a value ~ −60 km s^{-1} and extends to a radial distance ~64 kpc. The gas in the south-east direction extending to G4 (in the plane of the sky) does not seem to be associated with the galaxy: there is a large velocity difference (~1000 km s^{-1} — see below for the galaxy velocity) and no velocity distortion is apparent at the galaxy position.

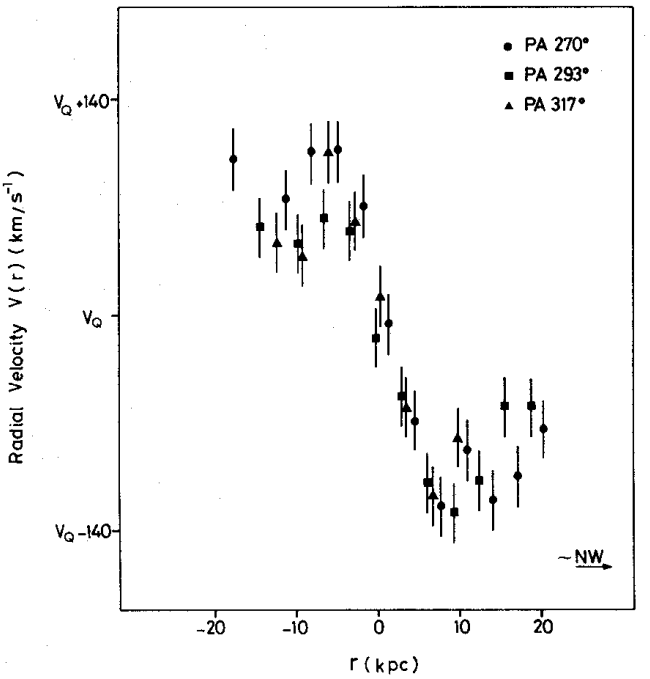

Figure 2. Rotation curves of the nebulosity close to MR 2251–178 at position angles 270°, 293° and 317°, obtained from the [O III] lines. The $\pm 1\sigma$ uncertainty in the velocity estimate is shown by the vertical bars. Velocities are referred to the QSO velocity $V_Q = 18568\,\mathrm{km\,s^{-1}}$.

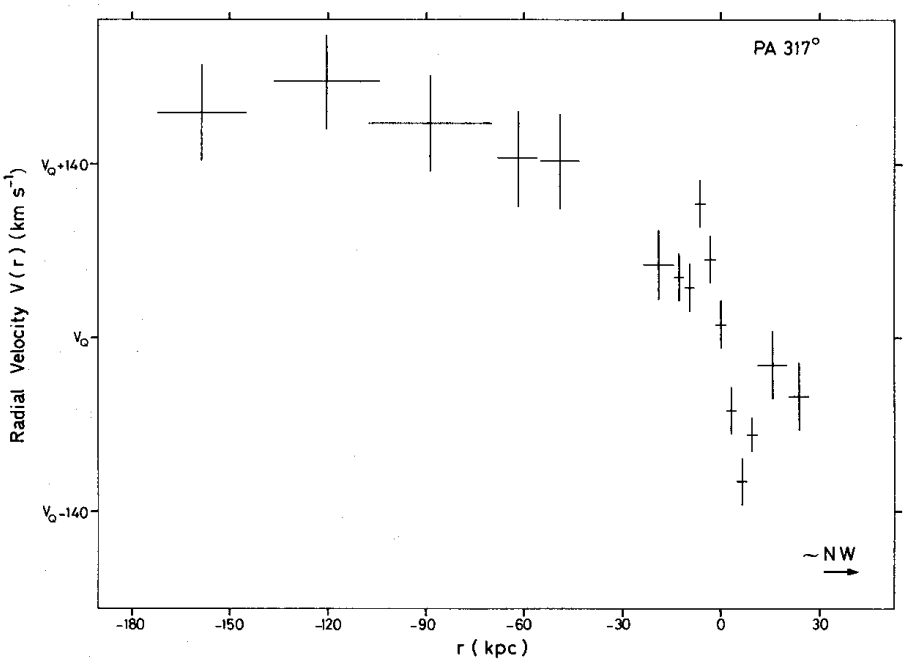

Figure 3. Rotation curve of the extended envelope in approximately the south-east to north-west direction as observed at position angle 317°, obtained from the [O III] lines. Velocities are as described in Fig. 2. The $\pm 1\sigma$ uncertainty in the velocity estimate is shown by the vertical bars and the extent over which adjacent spectrum strips are summed, by the horizontal bars.

A second emission region, not clearly attached to the main emission, but with comparable velocities, is evident ~90 kpc from the QSO and to the north of G2 (Plate 2). This could be part of the main envelope but our mapping of this region is very poor. We plan to study the QSO neighbourhood further.

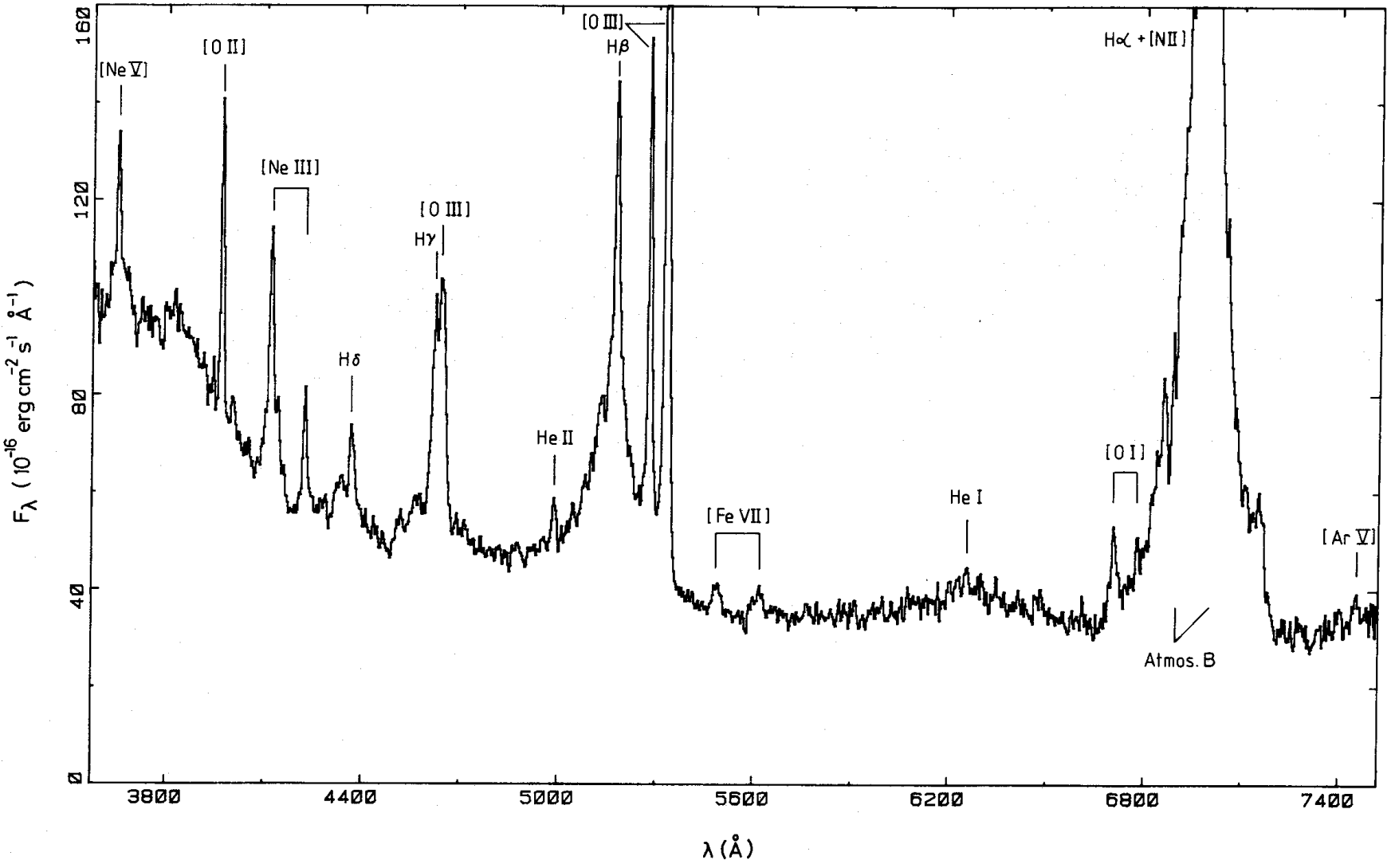

Figure 4. IPCS spectrum of MR 2251 −178, displayed on a scale of F_λ against observed wavelength. F_λ has been corrected as described in the text.

3.2 SPECTRA OF THE QSO AND NEBULOSITY

We obtained spectra of MR 2251–178 at the various position angles indicated in Plate 2; they are all qualitatively similar but only the one at 317° has a good signal-to-noise. In all cases the QSO spectra were extracted from a region 3 (across the slit) × 5.3 arcsec (along the slit) centred on the QSO. One additional exposure was made (at position angle 270°) with a GG 495 filter (cutting the blue part of the spectrum to exclude the overlapping second order) and with a different grating angle to extend our observations towards the red. This and our good unfiltered spectrum were joined at λ 5950. The overall spectrum appears in Fig. 4. It prominently shows a host of narrow emission lines and broad Balmer lines with narrow cores and, more weakly, He I and He II also with broad and narrow components. The observed lines are listed in Table 2.

The redshift of the QSO obtained from nine of the narrow emission lines is in good agreement with the value we determine from the [O III] rotation curves. The average is $z = 0.06398 \pm 0.00006$ (formally this is the vacuum, heliocentric value but the corrections are small). This is rather different from the average of the values given by Phillips (1980) but both are consistent with the less accurately determined value of Canizares *et al.* 1978). The discrepancy may come from the effect of beam-pulling in Phillips' SIT Vidicon observations, for which these devices are notorious under large signal conditions.

The continuous spectrum of the QSO shows a strong ultraviolet excess with an onset near $\lambda_0 4000$ (rest frame wavelength), in common with other low redshift QSOs (Baldwin 1975). Even ignoring this the continuum cannot be represented simply by a single power law, $F_\nu \propto \nu^{-\alpha}$, but a fitting with two slopes conforms reasonably well with the data, with $\alpha = 0$

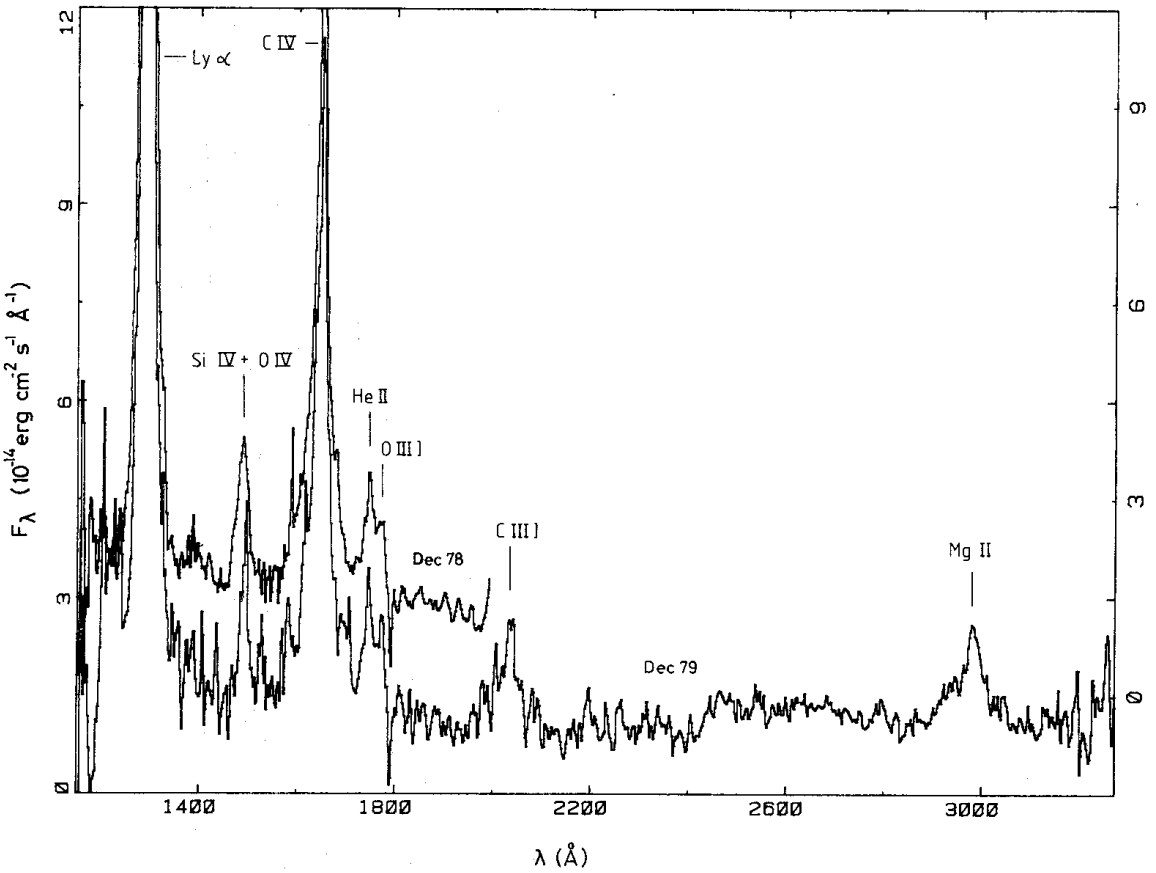

Figure 5. *IUE* spectrum of MR 2251 – 178 obtained in 1978 December (right F_λ scale) and 1979 December (left F_λ scale), displayed against observed wavelength. Note the right F_λ scale shift to avoid confusing the spectra.

over $\lambda_0\lambda_0$ 3400–4900 and $\alpha = 1.5$ over $\lambda_0\lambda_0$ 4900–7200. A comparison of infrared, optical and X-ray fluxes gives $\alpha = 1.2$ (Ricker *et al.* 1979). Coupled far-ultraviolet and optical observations are needed to define more precisely the spectral shape of the flat component. In an attempt to approach this, we have retrieved the following archival *IUE* observations: SWP 3730 of 1978 December (integration time, 180 min), three months after our optical observations and SWP 7486 with LWR 6570 of 1979 December (respective integration times, 35 and 150 min). These spectra are shown in Fig. 5 (note the scale shift to avoid confusion betweem the two epochs). The 1978 IPCS and *IUE* spectrum segments and continuum points extracted from the 1979 *IUE* spectra are compiled in Fig. 6. For the 1978 data, continuum points $\lambda_0\lambda_0$1350 and 5200 give $\alpha = 0.8$ but the spectrum clearly has more than one component: following the optical flat region the spectrum (1979 data) steepens strongly near $\lambda_0$2800 and hardens again ($\alpha \sim 0.4$ at both epochs) below $\sim\lambda_0$1800. In the year between the two SWP observations the intensity of the latter component decreased by (20 ± 3) per cent.

From our optical data we estimate the FWHM of the broad components of Hα and Hβ to be (6950 ± 250) km s^{-1}, larger than given by Canizares *et al.* (1978) although the full

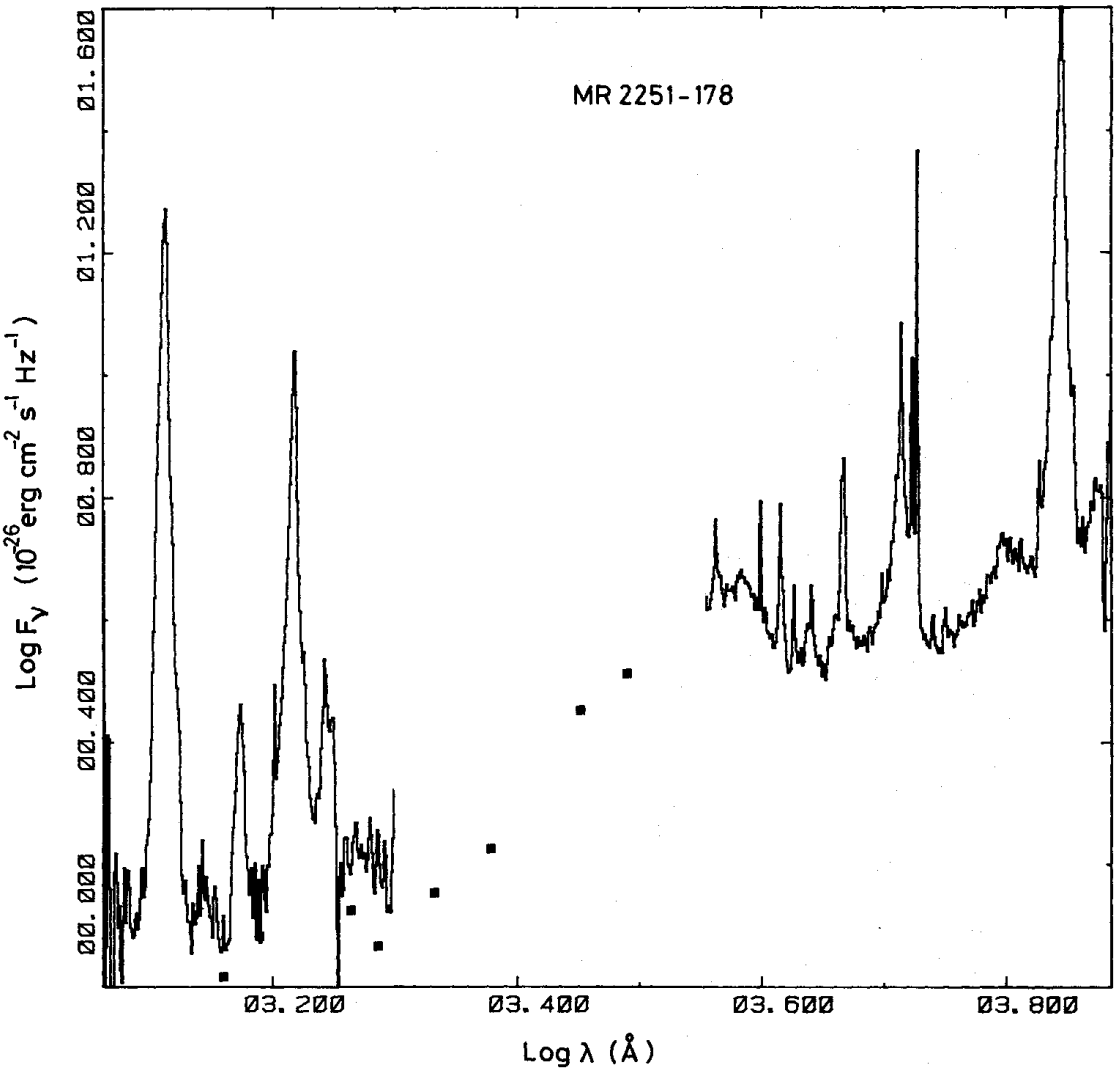

Figure 6. *IUE* (1978 December) and corrected IPCS (1978 September) spectra of MR 2251–178 displayed on a scale of log F_λ against log (observed wavelength). The filled squares are continuum points from the *IUE* 1979 December spectrum.

widths at zero intensity are similar to theirs. The blue wing of Hβ is slightly broader than for Hα and there may be some weak lines present. The *IUE* data yield 5500 km s^{-1} for the broad component of C IV (at both epochs) and Lyα (1979 only: in the 1978 spectrum Lyα is heavily saturated). The difference between the optical and far-ultraviolet line widths may not be significant since the low-resolution *IUE* data do not allow precise deblending of the broad and narrow components. The narrow [O II] and [O III] lines in the nucleus are resolved and have a FWHM of (490 ± 50) km s^{-1}, after correction for the instrumental profile.

Two weak lines in the blue wing of Hγ are identified with [Fe II] 21F λ4244 and 7F λ4287. Strong Fe II ultraviolet multiplets are present in the *IUE* data but are not associated with any detectable optical multiplets, as already found for intermediate redshift QSOs (Bergeron & Kunth, in preparation).

The total equivalent width of Hβ (broad and narrow components) as determined from our optical spectrum is (226 ± 9) Å. The observations of Canizares *et al.* (1979) were made in 1977 November with an aperture 3 × 6 arcsec oriented north–south, similar to our observations: we derive the value (152 ± 30) Å for Hβ from their data, assuming their continuum locally is at 4.0 mJy. The difference between the two values may arise from the choice of continuum (but even assuming a linear continuum in F_λ between $\lambda_0\lambda_0$4290–5060, which we believe to be higher than the true continuum, our value is still 201 Å), the estimate of the contribution of He II λ4686 to the blue wing of the Hβ (but the effect of this is small) or a real increase by 45 per cent from 1977 November to 1978 September. The ratio Hβ/[O III] apparently increased only 25 per cent over the same period. This suggests a possible simultaneous increase of both Hβ and continuum intensities. The *IUE* data show variations over a similar period. Between 1978 December and 1979 December, in addition to the continuum variation already mentioned, there was significant variation in some line strengths, as indicated in Table 3: the blend at $\lambda_0$1549 decreased by (18 ± 5) per cent, the blue wing of the blend at $\lambda_0$1397, corresponding to an unidentified line at $\lambda_0$1385, disappeared during 1979 (see Fig. 5) and N V λ1240, blended with Lyα, decreased by about a factor 2.

The Hα/Hβ ratios for the broad and narrow line regions of the QSO are 3.65 and 2.77 respectively. The latter is equal to the radiative recombination value and so implies there is little or no reddening in the line-of-sight to the narrow line region of the nucleus. The value 3.65 for the broad component is within the range of values observed for other active nuclei associated with weak compact radio sources. In the nebulosity (see below) the ratio Hα/Hβ is 3.66 and some extinction by dust, corresponding to $E(B-V) = 0.24$, may be present. The Lyα/Hβ ratios for the broad and narrow line regions of the QSO are 8 and 25 respectively, with an uncertainty > 50 per cent largely due to our optical photometric calibration (see below) and the difficulty of deblending. Wu, Boggess & Gull (1980) discuss Lyα/Hβ results for several Seyfert galaxies and MR 2251−178 but do not separate the broad and narrow line regions for the QSO.

Because of the poor photometric quality of our optical data our measured absolute fluxes are rather uncertain. However, we can derive a photometric correction factor from a comparison of our forbidden line fluxes with those given by Canizares *et al.* (1978) (accounting for their assumed correction for galactic extinction). These lines generally are known to be constant on a scale of years. We find a factor 2.11 from [O III] λλ4959, 5007. Phillips made spectrophotometric observations of MR 2251−178 in 1978 August 8, close in time to ours but with a slit width of 4 arcsec; although variation in the one month to our observations cannot be ruled out (Ricker *et al.* 1979) his 1978 November 7 data reassuringly are very similar. Comparing his August continuum levels with ours gives a factor 2.03. Accordingly we have applied a photometric correction factor of 2.1 to our spectra of the QSO and nebulosity (Figs 4, 6 and 7), but the combined uncertainties may amount to 50

Table 3. Far-ultraviolet lines of MR 2251 −178.

	Identification[a]	1978 December Flux[b] (10^{-14} erg cm^{-1} s^{-1})	1978 December Observed EW[b] (Å)	1979 December Flux[b] (10^{-14} erg cm^{-1} s^{-1})	1979 December Observed EW[b] (Å)
1216	Lyα (b)	790[c]	323[c]	695[d]	410
1216	Lyα (n)			185[d]	
1240	N V	35		17	
1304	OI	7		9	
1385		12[d]	33	~0	
1400	Si IV + O IV]	62 / 50[d]		42	24
1549	C IV(b) + Si II + [Ne V]	363[d]	213	295[d]	194
1549	C IV (n)	22[d]		23[d]	
1640	He II	34	18	36	24
1663	O III]	16		18	
1909	C III]			55	54
2280–2410	Fe II (UV 2 + 3 + 35 + 36)			63	67
2575–2640	Fe II (UV 1)			23	24
2740	Fe II (UV 62 + 63)			38	39
2798	Mg II			71	72

[a] Broad (b) and narrow (n) components are listed separately.

[b] The dominant uncertainty arises from placing the continuum and ranges from a few per cent for the stronger lines to ~ 30% for the weaker.

[c] This line is heavily saturated.

[d] Rough deblending only.

per cent. For the galaxy spectra (Fig. 8) we give only arbitrary units. We list our observed QSO and nebulosity (see below) line fluxes with the correction applied, in Table 2. Our corrected value for the Hβ flux corresponds reasonably well with the value given by Phillips (1980), in further support of the discussion earlier.

The line fluxes in the nebulosity were measured from the exposure made at slit position angle 346° running through G1 and north-east of the QSO (Plate 2). The nebulosity spectrum (Fig. 7) was extracted from a region 3 × 8.8 arcsec (5.6 × 16.6 kpc) whose centre lies 7 arcsec (13.2 kpc) away from the QSO and 38 arcsec (71 kpc) away from G1. The weak continuum has no strong ultraviolet excess and the emission lines are very narrow, implying no contamination from the nucleus. The continuum roughly can be fitted by a power law with $\alpha = 2.1$.

We carefully examined the nebulosity spectrum for the presence of absorption features. Although the signal-to-noise ratio in the continuum is poor, there are two unresolved absorption lines which we cannot attribute to interference from sky features, and identify as Ca II *K* and Mg I λ 5174, revealing the presence of an underlying galaxy with $z = 0.063 \pm 0.001$. The emission lines from the same region give $z = 0.0644 \pm 0.0001$. More observations are needed to determine the kinematics of the stars and confirm the different behaviour of the gas and stars.

The spectrum of the nebulosity is of much higher excitation than the region close to the nucleus (see Table 2). The ratio [O III] λλ 4959, 5007/Hβ increased from 4.7 at $r < 3.4$ kpc

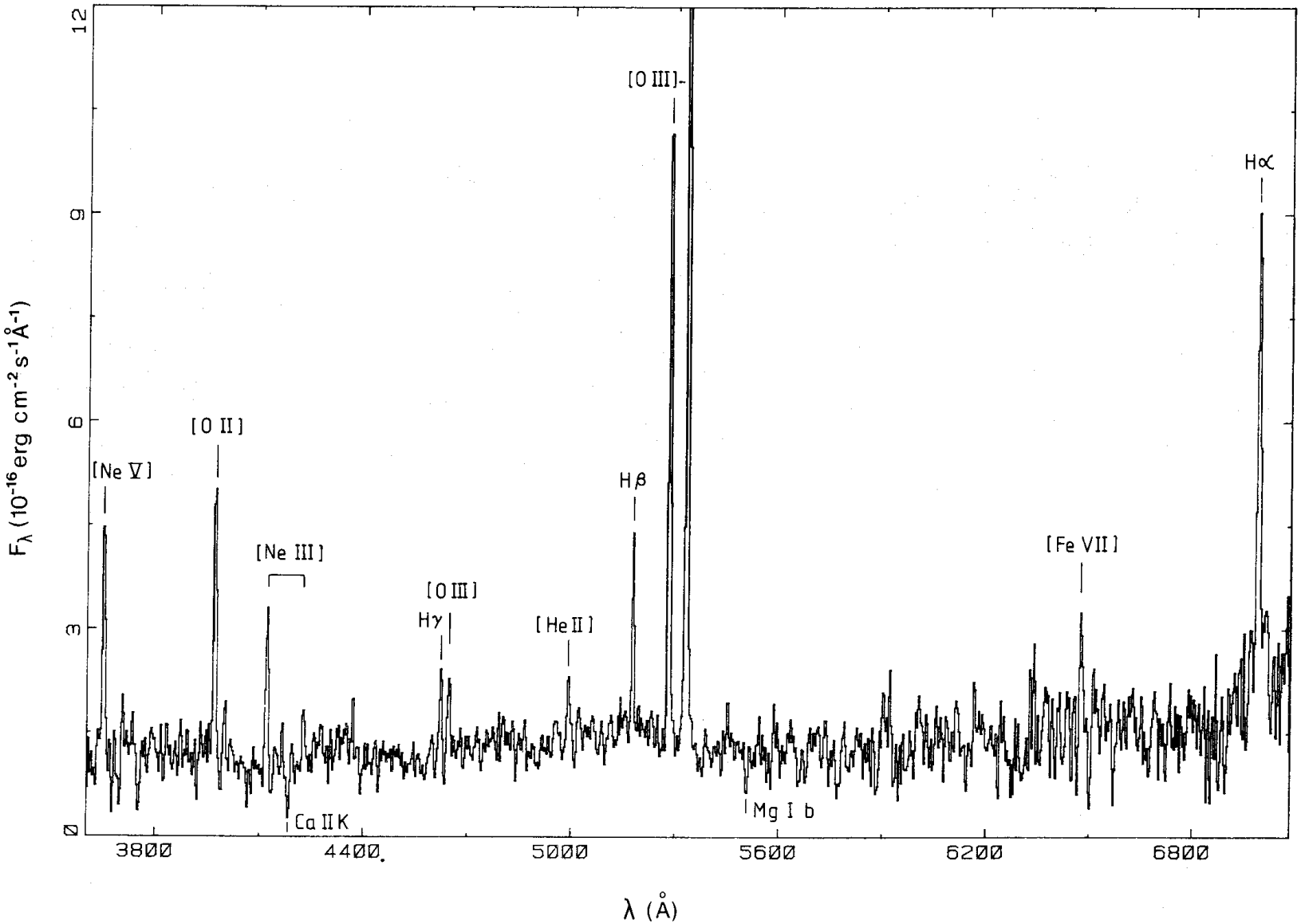

Figure 7. IPCS spectrum of the nebulosity extracted from a region 3 × 8.8 arcsec whose centre lies 7 arcsec away from the nucleus of MR 2251 −178 (see text), displayed as in Fig. 4 and similarly corrected.

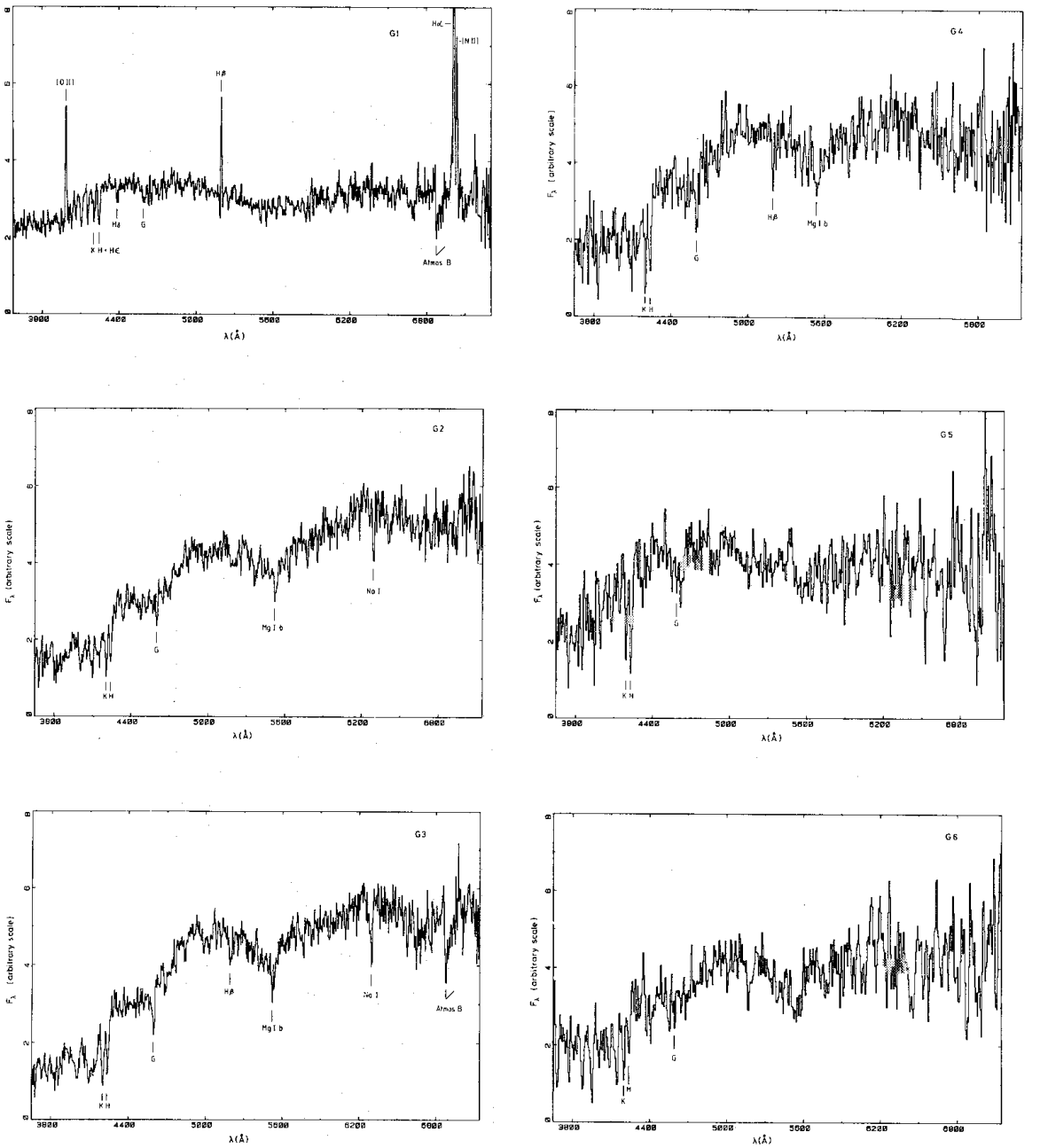

Figure 8. IPCS spectra of six galaxies (G1–G6) in the nearby field of MR 2251–178, displayed on an arbitrary scale in F_λ against observed wavelength. The noisier spectra have been smoothed over 3 pixels.

to 13.8 at $r = 13$ kpc and reaches 18 at $r = 20$ kpc. A stronger increase is found for the ratio [Ne V] λ3426/[Ne III] λ3869: from 0.5 in the nucleus to 1.5 at $r = 13$ kpc. The temperature in the nebulosity derived from the [O III] line ratio is $(3.0 \pm 0.3) \times 10^4$ K in the low density case; other ions may have a different temperature, particularly those of lower-ionization potential. Let us first consider the phase of higher excitation. The ionic abundances O^{++}/H^+, Ne^{++}/H^+ and Ne^{4+}/H^+ are respectively 2.9×10^{-5}, 5.7×10^{-6} and 8.7×10^{-6}. The spread in degree of ionization of Ne implies that a fair fraction of this element is in the form Ne^{3+} and Ne^{5+}, not detectable in the optical. Using results from models with coupled photoionization and heating equilibria and a power law photon spectrum (Bergeron, unpublished results) we derive an ionization correction factor of 2.0 for the overall abundance of

Ne and get Ne/H = 2.9×10^{-5}, a factor 4 lower than the cosmic abundance. Our ratio $O^{++}/Ne^{++} = 5.1$ is close to the cosmic value for O/Ne, indicating a similar underabundance for O and Ne. Although the [N II] lines are very noisy they are clearly present and, using the same temperature for the singly ionized elements as above, we find $O^{+}/N^{+} \sim 1$, much lower than the cosmic relative abundance O/N of 6. However, the low-excitation lines could be emitted by clumps of higher density and lower temperature than the highly excited region: for a temperature of 1×10^{4} K the ratio O^{+}/N^{+} would reach 2.5.

3.3 GALAXIES OF THE SURROUNDING CLUSTER

The spectra of the six galaxies observed with the IPCS, G1–G6, are given in Fig. 8. For the galaxies G7 and G8, observed with the IDS, only Hα in emission was detected. Emission lines also are strongly present in the spectrum of the compact galaxy G1, superposed on an absorption spectrum in the case of the Balmer lines; this galaxy is further discussed below.

Our observed radial velocities for the galaxies and QSO are collected in Table 4 (vacuum, heliocentric values). Our velocity differences between G1–G4 and the QSO are systematically higher than Phillips' (1980) values and we have already noted a significant discrepancy between his and our redshift for the QSO. However, from his given values (and allowing for his correction for galactic rotation) we find his galaxy velocities conform much better with ours than do his listed differences, confirming that the discrepancy lies substantially in his value for the QSO velocity.

The average velocity of the cluster, v_0, obtained from the values listed in Table 4 is $(19\,393 \pm 155)\,\mathrm{km\,s^{-1}}$; in column 3 we list differences from v_0. The QSO both is highly off-central in the cluster and has a radial velocity in the low-velocity tail of the cluster velocity distribution. The velocity dispersion of the cluster is $396\,\mathrm{km\,s^{-1}}$ and reduces to $283\,\mathrm{km\,s^{-1}}$ (and v_0 increases $19\,496\,\mathrm{km\,s^{-1}}$) if the QSO is excluded. In both cases the velocity distribution is roughly consistent with a Gaussian distribution of the same velocity dispersion. The FWHM of the Gaussian distribution with the QSO included is $930\,\mathrm{km\,s^{-1}}$, which is ~3 times larger than the observed velocity spread in the extended envelope.

Table 4. Radial velocities.

Object	v [a] (km s^{-1})	$v - v_0$ [a,b] (km s^{-1})
MR 2251-178	18568 ± 20	-825
G1	19814 ± 40	421
G2	19473 ± 130	80
G3	19261 ± 70	-132
G4	19747 ± 70	354
G5	18964 ± 225	-429
G6	19666 ± 225	273
G7	19291 ± 280	-102
G8	19753 ± 280	360

[a] All velocities (v) are vacuum, heliocentric values.

[b] The velocity v_0 is the average from column 2: 19393 km s^{-1}.

The question of cluster membership for the QSO can also be approached from a consideration of the effect on the interstellar gas in the apparently close galaxy G1 of the hard photons from the QSO already responsible for heating the extensive H II envelope. The galaxy emission line spectrum is of low excitation, with [O III] λ 5007/Hβ ~ 1/7 and [O II] λ 3727/Hβ ~ 1.2; it resembles H II region spectra of low excitation with electronic temperatures of order 7000 K. If the true distance, d, between the QSO and G1 is close to the projected distance, ~ 75 kpc and assuming the envelope is optically thin to the QSO hard ultraviolet radiation, the interstellar matter in the galaxy would be more ionized ([O III] λλ 4959, 5007 ≳ [O II] λ 3727) than observed, for interstellar densities $n \lesssim 10\,\mathrm{cm}^{-3}$ (Bergeron, unpublished results). The gas density would be closer to average interstellar densities ($n \sim 1\,\mathrm{cm}^{-3}$) if d were greater. Since the degree of ionization is proportional to $(nd^2)^{-1}$, $d \gtrsim 5$ times the projected distance is compatible with a low-density interstellar gas and the QSO then could still be well within the cluster.

Diffuse X-ray emission from the cluster is not very likely on statistical grounds (McKee *et al.* 1980) since the number of galaxies belonging to the cluster is small, about 50 (Phillips 1980) and the cluster is of BM type III. However, the motions of the surrounding galaxies through the H II envelope may induce some increase in the gas temperature if the envelope is within the cluster core radius. A hot X-ray component may exist if a low-density phase ($n \sim 3 \times 10^{-4}\,\mathrm{cm}^{-3}$) is present, heated both by the galaxy motions and the X-ray photons from the QSO.

A faint object, marked G9 in Plate 2, lies 18.5 arcsec south-west of the QSO in the direction of galaxy G4. Its spectrum shows a faint continuum, with signal-to-noise ratio too low to detect absorption features and a few narrow emission lines identified with [O II], [Ne III], Hβ and [O III]. The redshift is 0.121 ± 0.001 and the line intensities relative to Hβ are 2.5, 1 and 3.5 for [O II] λ 3727, [Ne III] λ 3896 and [O III] λ 5007 respectively. This faint object is probably a background galaxy. Similar objects in size and magnitude can be seen in Plate 1.

4 Discussion

Only a few H II nebulosities associated with active nuclei have been studied spectro-spatially. Their velocity fields strongly differ and no general scheme can be given. Highly disordered motions are present in the nebulosity around 3C 120 but some rotation is discernible at a position angle roughly aligned with the axis of the compact expanding radio source (Baldwin *et al.* 1980). A clear rotation pattern is observed in the radio elliptical galaxy PKS 2158−380, but the stars do not rotate at all about the rotation axis of the gas, which may suggest that the gas has been accreted (Fosbury *et al.* 1982); furthermore, there is no alignment between the radio axis of the components of the extended radio source and the gaseous rotation axis.

We have found that the gas around the nucleus of MR 2251−178 most likely rotates about an axis having a position angle within the range 270–320°. A velocity gradient of $17\,\mathrm{km\,s^{-1}\,kpc^{-1}}$ exists at radius $r < 6$ kpc. Further out the rotation curve is not symmetrical and for the observed maximum extension the rotation velocity remains substantially constant at $180\,\mathrm{km\,s^{-1}}$ relative to the nucleus over a large distance, at least to 170 kpc. From this, on the assumption of circular motions, we can derive the total mass within a radius of 170 kpc and obtain $M_{\mathrm{total}} = 1.3 \times 10^{12}/\sin^2 i\, M_\odot$, where i is the unknown inclination angle. This large mass is within the upper range found for Seyfert galaxies from an H I survey (Heckman, Balick & Sullivan 1978).

As for PKS 2158−380, our observations suggest that the gas and stars of the nebulosity around MR 2251−178 do not have the same velocity field. The morphology of the galaxy

underlying the QSO is unknown. An elliptical galaxy is not required by the radio properties of the QSO, which is only a weak compact radio source.

The continuity of the velocity field strongly favours an association of all the ionized gas with the QSO, but this could be either the interstellar matter of the galaxy or accreted material, or both. In the nebulosity the underabundance of heavy elements by a factor 4, at a radial distance of 13 kpc, may indicate a different star formation history than in normal galaxies. For the extended envelope, an estimate of the gaseous mass and its ratio to the total mass may shed some light on the nature of this component.

In the nebulosity close to the QSO, $6 < r < 15$ kpc, we may determine the gas column density from the observed Hβ flux using the temperature derived from the [O III] line ratio. The average density, $\langle n \rangle$, can be roughly derived if an estimate of the dimensions along the line-of-sight, l, can be made. The value for l is a function of the inclination and the disc geometry. The nebulosity seems fairly circular on photographic plates, suggesting it is viewed far from edge-on and we use $l = 10$ kpc. We find:

$$nl = 1 \times 10^{21} n^{-1} \text{ cm}^{-5},$$

$$M = 4 \times 10^{9} n^{-1} M_{\odot},$$

and

$$\langle n \rangle \sim 0.3 \text{ cm}^{-3}.$$

From the presence of [O II] and [S II] lines and our very approximate ratio [S II] λ6717/[S II] λ6731, we place an upper limit of 300 cm^{-3} on the electronic density of the low-excitation phase, implying $M > 10^{7} M_{\odot}$.

Another estimate of the ionized gas density can be derived from the degree of ionization, on the assumption of photoionization by the hard radiation source of the QSO. In the optically thin case and ultraviolet power-law spectrum $F_{\nu} \propto \nu^{-1}$, a two phase model is needed for the nebulosity. The lower density phase in which the higher excitation lines ([O III], [Ne III] and [Ne V]) are formed must have a density of order 15 cm^{-3} at $r = 12$ kpc (Bergeron, unpublished results). The high temperature follows from the underabundance of heavy elements. If the narrow line region associated with the nucleus is optically thick in the Lyman continuum and has a large covering factor, only soft X-ray photons will reach the nebulosity. For a low energy cut-off at $h\nu_{\text{min}} \sim 200$ eV, the nebulosity emission line spectrum is compatible with a single phase of density $n \sim 1$ cm^{-3} (see, e.g., Tarter, Tucker & Salpeter 1969).

The mass of ionized gas in the nebulosity is $4 \times 10^{8} < M_{\text{H II}} < 2 \times 10^{10} M_{\odot}$. This emissive region can be the interstellar matter of a spiral galaxy, ionized by the hard radiation from the active nucleus.

In the extended envelope only the [O III] lines are detected. A rough estimate of nl and M can be obtained by assuming the same temperature and O^{++}/H^{+} ratio throughout the envelope as in the outer nebulosity. If the O^{++}/O ratio were a decreasing function of distance from the QSO our estimate for the mass would be only a lower limit. We know neither the total extent of the envelope, nor its geometrical shape. We assume for the dimension along the line-of-sight a value $l = (230 \times 60)^{1/2}$ kpc and get for the envelope within a projected area of 230×60 kpc^2:

$$nl = 4 \times 10^{19} n^{-1} \text{ cm}^{-5},$$

$$M = 4 \times 10^{9} n^{-1} M_{\odot},$$

and

$$\langle n \rangle \sim 1 \times 10^{-2} \text{ cm}^{-3}.$$

An estimate of the density in the envelope can only be derived from ionization equilibrium arguments. Since Hβ is not detected the degree of ionization remains high throughout the envelope and we assume a ratio [O III] λλ 4959, 5007/Hβ as in the outer nebulosity. We find from the ionization equilibrium at $r = 100$ kpc densities of 0.3 and 0.03 cm^{-3} for $h\nu_{min}$ = 13.6 and 200 eV respectively. The latter alternative would arise either if the gas in the nucleus were optically thick to the Lyman continuum, or if the density in the nebulosity were close to 15 cm^{-3}. The mass of the extended envelope is $2 \times 10^{10} < M_{H\,II} < 5 \times 10^{11} M_{\odot}$.

The opacity, τ, of the nebulosity and the envelope in the soft X-ray range can be estimated for comparison with observations by the *Einstein* X-ray satellite (not yet fully analysed: Kriss, private communication). In this range ($h\nu > 600$ eV) τ is a function of He^+ and O. From the ionization equilibrium in the nebulosity we find $He^+/He \sim 0.3$ and τ (600 eV) is then mainly a function of He^+ since O is underabundant. This opacity remains smaller than unity in the nebulosity whatever its density. It is of order unity in the envelope for $n = \langle n \rangle = 1 \times 10^{-2}$ cm^{-3}.

The power radiated by the QSO is far greater than the energy losses in the H II envelope. The [O III] λ 5007 luminosity is 2.6×10^{42} erg s^{-1} in the extended envelope. For a power law $F_\nu \propto \nu^{-1}$ the energy emitted by the QSO in one energy decade is 1.3×10^{45} erg s^{-1} (derived from the observed optical continuum at λ 5000). As the [O III] optical lines represent around 10 per cent of the energy losses of the gas, only 5 per cent of the ionizing flux from the QSO is absorbed in the whole H II envelope. This implies either a small spatial coverage or an optically thin medium.

The H II envelope around MR 2251−178 and X-ray emitting gas in small groups of galaxies (Schwartz, Schwarz & Tucker 1980) are of similar extent but the mass of hot X-ray gas reaches 10^{12}–$10^{13} M_{\odot}$, larger than our estimate for the envelope. However, the mass of the H II envelope does fall within the range of masses for H I envelopes around Seyfert nuclei (Heckman *et al.* 1978). A neutral envelope of 200 × 300 kpc is observed around the Seyfert galaxy Mk 348 and its rotation curve is still rising out to at least 100 kpc (Morris & Wannier 1980). The mass of this H I envelope is $3 \times 10^{10} M_{\odot}$. Neutral gas may be associated with the H II envelope around MR 2251−178 and the QSO should be observed at 21 cm. A possible difference for Mk 348 is its weak X-ray power ($L_x/L_{opt} \sim 1/100$: Kriss, Canizares & Ricker 1980); it is also intrinsically less luminous ($L_{opt} = 4 \times 10^{43}$ erg s^{-1}).

Extended H II nebulosities associated with broad-line active nuclei are not common, as we are finding from our continuing survey and the only ones detected at present are associated with very bright nuclei. They may occur more frequently in narrow line radio galaxies (Fosbury, private communication), although a few cases only are known. Small H II nebulosities (radii of a few kpc) are seen around a few Seyfert 1 galaxies, like NGC 3516 (Ulrich & Pequignot 1980), but occur more often around Seyfert 2 galaxies (Balick & Heckman 1979, and our survey). Coupled 21-cm and optical observations are needed to see whether an important factor, besides the opacity of the broad-line region, may be the distribution of the interstellar gas.

5 Acknowledgments

We thank the technical support group on La Silla for their help in installing the UCL travelling IPCS on the 3.6-m telescope. As usual, particular thanks are due to John Fordham and Keith Shortridge for continuing improvements to the IPCS and for their invaluable and unstinting work in setting it up and cheerfully maintaining it over the observing run. We gratefully thank W. L. W. Sargent for encouragement and very helpful discussions. The IPCS was developed with the aid of grants from SERC.

References

Baldwin, J. A., 1975. *Astrophys. J.*, **201**, 26.

Baldwin, J. A., Carswell, R. F., Wampler, E. J., Smith, H. E., Burbidge, E. M. & Boksenberg, A., 1980. *Astrophys. J.*, **236**, 388.

Balick, B. & Heckman, T., 1979. *Astrophys. J.*, **84**, 302.

Boksenberg, A., 1978. *Proc. of the ESO Conference, Optical Telescopes of the Future, December 12–15, Geneva*, p. 497.

Canizares, C. R., McClintock, J. E. & Ricker, G. W., 1978. *Astrophys. J.*, **226**, L1.

Cooke, B. A., Rickets, M. J., Maccacaro, T., Pye, J. P., Elvis, M., Watson, M. G., Griffiths, R. E., Pounds, K. A., McHardy, I., Maccagni, D., Seward, F. D., Page, C. G. & Turner, M. J. L., 1978. *Mon. Not. R. astr. Soc.*, **182**, 489.

Fairall, A. P., 1979. *Mon. Not. R. astr. Soc.*, **188**, 343.

Fosbury, R. A. E., Boksenberg, A., Snijders, M. A. J., Danziger, I. J., Disney, M. J., Goss, W. M., Penston, M. V., Wamsteker, W., Wellington, K. & Wilson, A. S., 1982. preprint.

Gunn, J. E., 1971. *Astrophys. J.*, **164**, L113.

Heckman, T. M., Balick, B. & Sullivan III, W. T., 1978. *Astrophys. J.*, **224**, 745.

Kriss, G. A. Canizares, C. R. & Ricker, G. R., 1980. *Astrophys. J.*, **242**, 492.

Kristian, J., 1973. *Astrophys. J.*, **179**, L61.

McKee, J. D., Mushotzky, R. F., Boldt, E. A., Holt, S. S., Marshall, F. E., Pravdo, S. H. & Serlemitsos, P. J., 1980. *Astrophys. J.*, **242**, 843.

Morris, M. & Wannier, P. G., 1980. *Astrophys. J.*, **238**, L7.

Oke, J. B., 1974. *Astrophys. J. Suppl. Ser.* **27**, 21.

Phillips, M. M., 1980. *Astrophys. J.*, **236**, L45.

Ricker, G. R., Clarke, G. W., Doxsey, R. E., Dower, R. G., Jernigan, J. G., Delvaille, J. P., MacAlpine, G. M. & Hjellming, R. M., 1978. *Nature*, **271**, 35.

Ricker, G. R., Clarke, G. W., Doxsey, R. E., Dower, R. G., Jernigan, J. G., Canizares, C. R., Delvaille, J. P. MacAlpine, G. M. & Hjellming, R. M., 1979. *X-ray Astronomy*, p. 281, eds Baity, W. A. & Peterson, L. E., Pergamon, Oxford.

Schwartz, D. A., Schwarz, J. & Tucker, W., 1980. *Astrophys. J.*, **238**, L59.

Stockton, A., 1976. *Astrophys. J.*, **205**, L113.

Stockton, A., 1978. *Astrophys. J.*, **223**, 747.

Tarter, C. B. Tucker, W. H. & Salpeter, E. E., 1969. *Astrophys. J.*, **156**, 943.

Ulrich, M.-H. & Pequignot, D., 1980. *Astrophys. J.*, **238**, 45.

Wampler, E. J., Robinson, L. B., Burbidge, E. M. & Baldwin, J. A., 1975. *Astrophys. J.*, **198**, L49.

Worral, D. M., Boldt, E. A., Holt, S. S. & Serlemitsos, P. J., 1980. *Astrophys. J.*, **240**, 421.

Wu, C. C., Boggess, A. & Gull, T. R., 1980. *Astrophys. J.*, **242**, 14.

Wyckoff, S., Morton, D. C., Boksenberg, A. & Albrecht, R., 1980b. *Astrophys. J.*, **242**, L59.

Wyckoff, S., Wehinger, P. A. & Gehren, T., 1981. *Astrophys J.*, **247**, 750.

Wyckoff, S., Wehinger, P. A., Spinrad, H. & Boksenberg, A., 1980a. *Astrophys. J.*, **240**, 25.